

See discussions, stats, and author profiles for this publication at: <https://www.researchgate.net/publication/243374456>

Pd-Supported Interaction-Defined Selective Redox Activities in Pd–Ce_{0.7}Zr_{0.3}O₂–Al₂O₃ Model Three-Way Catalysts

ARTICLE *in* THE JOURNAL OF PHYSICAL CHEMISTRY C · JULY 2009

Impact Factor: 4.77 · DOI: 10.1021/jp810904d

CITATIONS

18

READS

22

7 AUTHORS, INCLUDING:



Ming Yang

General Motors Company

13 PUBLICATIONS 190 CITATIONS

[SEE PROFILE](#)



Jun Wang

The Chinese University of Hong Kong

694 PUBLICATIONS 15,261 CITATIONS

[SEE PROFILE](#)

Pd-Supported Interaction-Defined Selective Redox Activities in Pd–Ce_{0.7}Zr_{0.3}O₂–Al₂O₃ Model Three-Way Catalysts

Ming Yang,[†] Meiqing Shen,^{*,†,‡} Jun Wang,[†] Jing Wen,[†] Minwei Zhao,[†] Jie Wang,[†] and Wulin Wang[§]

Key Laboratory for Green Chemical Technology of State Education Ministry, School of Chemical Engineering & Technology, Tianjin University, Tianjin 300072, PR China, State Key Laboratory of Engines, Tianjin University, Tianjin 300072, PR China, and China Automotive Technology & Research Center, Tianjin 300162, PR China

Received: December 10, 2008; Revised Manuscript Received: June 2, 2009

Effects of Pd-supported interactions toward redox behaviors concerning three-way catalytic reactions and oxygen-buffering effects are investigated through stepwise changing Pd-loading locations over ceria–zirconia and alumina. Through light-off tests and kinetics, texture, and surface studies, discrepant but redistributable Pd–Al₂O₃ and Pd–Ce_{0.7}Zr_{0.3}O_x interfaces are defined and analyzed. Pd species are inclined to promote the transformation of Ce⁴⁺ to Ce³⁺ and maintain themselves as fine particles on ceria–zirconia surfaces. Oxygen spillover promoted by Pdⁿ⁺/Pd⁰–Ce⁴⁺/Ce³⁺ redox couples benefits the oxygen-buffering effect, but is limited by the increase of reaction temperatures and ceria–zirconia reducibility. This strong oxidative interaction overcomes the possibility of ceria-related anionic vacancies in facilitating NO dissociation and, thus, improves CO conversion only. Stochiometric light-off tests show higher activities for NO reduction and C₃H₈ oxidation on a Pd–Al₂O₃ interface, where the different morphologies and redox states of Pd-supported interfaces should be the main contributing factors for efficient molecular bond dissociation.

1. Introduction

Three-way catalysts (TWCs) have been widely applied for exhaust control of gasoline automotives, converting CO, C₃H₈, and NO_x into CO₂, H₂O, and N₂ via redox reactions.¹ TWCs are composed of mainly three parts, including active noble metals (NM, such as Pt, Rh, and Pd) serving as the main sites for molecular activation, support oxides providing high surface areas, and ceria-related materials as promoters.² Ceria–zirconia displays sustain higher metal dispersion,³ stabilize the γ-Al₂O₃ phase at a high surface area,⁴ and promot a water–gas shift (WGS) reaction.⁵ Noticeably, because the oxygen storage capacity (OSC) originated from the chemical transmission between Ce⁴⁺ and Ce³⁺,⁶ ceria-based materials can serve as oxygen buffering materials in attenuating the fluctuation of the air/fuel (A/F) ratio of ~14.6 during engine operations.

Textural defects of ceria-based oxides possibly contribute to OSC.^{7,8} However, the overall catalytic performance could neither be absolutely dictated by the OSC activity of ceria-related materials⁹ nor the NM particles.¹⁰ Studies focused on interactions among the three standard components in modifying TWC activity have drawn great attention.^{11,12} The spillover effect and strong metal–support interaction (SMSI) are of great importance to the principal steps of the catalytic process such as adsorption, surface and bulk reactions, and desorption. Cost-effective Pd-only catalysts were applied in TWCs, where the Pd–Ce contact enhanced NO conversion by facilitating N–O dissociation.¹³ Ranga Rao et al.¹⁴ claimed a better NO conversion in a CO + NO reaction. The oxygen vacancies formed during a Pd–Ce interaction, which activated free electrons, contributed to this.

Martínez-Arias et al.^{15,16} reported that Pd–Al₂O₃ also exerts a desirable performance for NO reduction. They deduced that the Pd geometrical and electronic states affected by Al₂O₃ would contribute to NO conversion, and the anionic vacancy-rich ceria–zirconia patches on alumina may serve as a kind of practical additive for NO_x dissociation. Even for the complex situation of the synchronous conversion of CO, NO, and HC_s, ambiguity concerning the desirable Pd chemical states and Pd-supported interactions still exist.^{17–20} Further justification for the oxidative or reductive Pd-supported interfacial effect under specific situations may be appealing.

To evaluate the oxygen buffering effect, which is important to real applications, we applied a dynamic oxygen storage capacity (DOSC) measurement by exposing catalysts to sequential pulses of CO, He, and O₂, simulating the oscillating rich and lean conditions.²¹ OSC performances related to intrinsic ceria–zirconia structures were widely discussed,¹ while the impact of Pd-supported interactions seems more dominating for DOSC performances. Descorme et al.²² investigated the DOSC behavior under 1 Hz transient CO–O₂ pulses and found the interaction between palladium and ceria–zirconia facilitating the DOSC performance. Efsthathiou et al.²³ studied the static reduction behaviors of the catalysts similar to commercial formulations, where Pd–Rh was loaded on closely combined Ce_xZr_{1-x}O₂–Al₂O₃ support oxides. They found the deterioration of OSC is a consequence of the loss of metal surface area due to decreased interfacial contact between metal and ceria–zirconia during thermal aging. In their work, the NM-supported interfaces characterized by OSC activity were also expected to correlate with the performance of the TWCs to some extent.

* To whom correspondence should be addressed. E-mail: mqshen@tju.edu.cn.

[†] School of Chemical Engineering & Technology, Tianjin University.

[‡] State Key Laboratory of Engines, Tianjin University.

[§] China Automotive Technology & Research Center.

Perusal of the literature shows the importance of redox activity induced by Pd-supported interactions for exhaust control, but the definite behavior of the interfacial effect needs further addressing. In order to avoid the modifications induced by

ceria–alumina contacts,^{24,25} Pd–Ce_{0.7}Zr_{0.3}O₂–Al₂O₃ model catalysts were investigated through stepwise changing Pd-loading locations over ceria–zirconia and Al₂O₃ particles. The present work aims to provide further discussion on the factors determining the functions of Pd–Ce_{0.7}Zr_{0.3}O₂ and Pd–Al₂O₃ interfaces as oxygen buffers and key catalytic redox components for TWCs. Performance, kinetics, and surface and bulk studies are conducted to study their roles in model reactions.

2. Experimental Section

2.1. Sample Preparation. Ce_{0.7}Zr_{0.3}O₂ was synthesized by coprecipitation. Ce(NO₃)₃- and ZrO(NO₃)₂-mixed solutions in distilled water were added to ammonia under vigorous stirring and ending at pH ~9. The precipitator was deposited at 70 °C for 12 h. The filtered precipitates were subsequently calcined at 773 K for 5 h to obtain Ce_{0.7}Zr_{0.3}O₂ (CZ) powder. γ-Alumina (A) was prepared by a similar method with an Al(NO₃)₃ solution.

Pd-supported samples with a loading ratio of 0.5 wt % were obtained by incipient wetness impregnation with Pd(NO₃)₂. Five samples with stepwise changing Pd-loading locations were designed and designated as Pd/CZ, (Pd/CZ) + A, (Pd/CZ) + (Pd/A), (Pd/A) + CZ, and Pd/A on the basis of the notion of chromatogram-distributing Pd species between ceria–zirconia and alumina. The weight ratio of CZ to Al₂O₃ powder was 1:1 in the samples with mixed support oxides. In the case of the (Pd/CZ) + A catalyst, a Pd (NO₃)₂ solution was exclusively preimpregnated on CZ, followed by drying at 393 K overnight, and calcination at 773 K for 3 h. The (Pd/CZ) + A catalyst was obtained by mechanically mixing as-prepared Pd/CZ and Al₂O₃ powder. For the (Pd/A) + CZ catalyst, all of the Pd (NO₃)₂ solution was preimpregnated on the Al₂O₃ powder. Following the procedure, the (Pd/A) + CZ catalyst was obtained by mechanically mixing CZ and Pd/Al₂O₃ powder. In the case of the (Pd/CZ) + (Pd/A) catalyst, the same amount of Pd (NO₃)₂ was impregnated on the CZ and Al₂O₃ powders before mixing them together. Aged samples were obtained by hydrothermally aging the as-prepared catalysts at 1223 K for 10 h in a 10% steam–air condition.

2.2. Characterization. BET surface areas were measured by N₂ adsorption with a Quanta chrome NOVA 1200 apparatus. Samples were degassed under flowing N₂ gas at 473 K for 2 h before testing.

Powder X-ray diffraction (XRD) patterns were acquired with an Rigaku D/max 2500 diffractometer operating at 40 kV and 200 mA with nickel-filtered Cu Kα radiation and ranging from 10° to 90° with a 0.02° step size. Lattice constants were determined on the basis of Bragg's law, $2d \sin \theta = k \lambda$, with JADE 5.0.

H₂ chemisorption at 298 K was conducted on Micromeritics AutoChem 2910. Significant errors of metal accessibility can be minimized by having a (i) moderate reduction temperature for depressing SMSI and (ii) low H₂ pressure to forbid palladium hydride formation and exclude the H₂ spillover effect.^{26,27} Studies show that notorious palladium hydride formation is more favorable for larger Pd particles²⁸ and H₂ concentrations of 5–10% in 1 atm.²⁹ The present work followed those methods proposed by previous work measuring NM dispersion of NM-supported catalysts by H₂ chemisorption.^{27,30} Samples were preheated in He to 623 K, oxidized in O₂ at 623 K for 10 min, and subsequently purged with He at 673 K for 10 min. The sample is then reduced in H₂ at 673 K for 2 h and subsequently purged with He (keeping at 673 K for 10 min) to 298 K. The apparent equilibrium was approached when the pressure change was less than 0.01% for five readings taken at 30 s interval. A

range of H₂ pressure of 2–18 Torr (two torr steps) was used. Adsorbed volumes were determined by extrapolation of the linear part of the adsorption isotherm to zero pressure. A chemisorption stoichiometry of H:NM = 1:1 was assumed.

Diffuse reflectance infrared Fourier transform spectroscopy (DRIFTS) studies were conducted on a Nicolet6700 FTIR with a MCT detector, using OMNIC software. In situ reaction studies were conducted with a 1073 K vacuum chamber (Thermofisher) fitted with ZnSe windows. Specific instructions for each experimental procedure are introduced below each group of spectra, including CO DRIFTS under vacuum system, CO DRIFTS in gas flow, and CO–NO–O₂ DRIFTS in gas flow. Spectra were collected at the resolution of 4 cm^{−1} and 32 scans with a heating rate of 5 K min^{−1}. All backgrounds were collected before the start of the adsorptions and heating from room temperature. Contributions of CO (g) bands were subtracted from all CO DRIFTS spectra. CO (g) spectra, where the CO concentrations were the same as those applied in situ characterizations, were collected at 303 K, using IR grade KBr placed in a sample cell.

2.3. Reaction Test. Two types of OSC measurements were conducted, including dynamic CO–He pulses and CO–O₂ pulses.^{7,25} Concentrations of CO, O₂, CO₂, Ar, and He in the outlet gas were monitored online by a Hiden HPR20 quadrupole mass spectrometer. A twenty-five milligram sample diluted with 40 mg of quartz sand was placed in the heat transfer reactor (10 mm diameter) at a height of 1.5 mm, with additional 4 mm redistributing layers of quartz wool on the two sides of the catalyst bed. The flow rate of every pulse is 300 mL min^{−1}. The dead volume of the system was 3.5 mL. Errors induced by residence time and possible CO + O₂ turbulent mixing involving catalytic combustion can be limited to 2% during OSC quantifications.

The two experimental modes are described as follows. (1) Transient oxygen release measurements at 773 K were conducted under consecutive CO (5 s)–He (40 s) conditions, and 4% CO/1% Ar/He and He were alternately pulsed for 10 times in sequence. (2) Dynamic CO–O₂ pulse (DOSC) measurements were operated from 473 to 773 K, and 4% CO/1% Ar/He and 2% O₂/1% Ar/He were pulsed alternately in sequence at the frequency of 0.1 and 0.05 Hz as simulated plug flows for more than 10 cycles to guarantee the reproducibility of collected response curves. Before both of the testing modes, samples were preoxidized under a 2% O₂/1% Ar/He atmosphere and then purged under He until no ³⁶O₂ signal was detected.

TWC light-off tests at a stoichiometric A/F ratio of $\lambda = 1$ used a gas mixture of 7% steam + 2% CO + 0.1% C₃H₈ and 0.1% NO + 1.45% O₂ + 12% CO₂ (N₂ balance gas) at a space velocity of 50000 h^{−1}. Four hundred milligrams of a catalyst diluted by quartz sand to 1.8 mL was placed at the bottom of quartz reactor. A standard test consisted of increasing the temperature from 373 to 873 at 15 K min^{−1}. Concentrations of CO, CO₂, NO, and C₃H₈ were quantified by an IR detector.

3. Results

3.1. Texture Analysis. The stepwise change of Pd locations on different supports modifies the morphology of NM particles and the structure of CZ supports on the different Pd-supported interfaces (Table 1). The absence of Pd features in XRD patterns (Figure 1) is attributed to 0.5 wt % low loading ratios. Discrepant Pd dispersions range from 16–75% and agree with the published result.^{27,30} Pd particles on CZ generally stay as more fine particles, compared with the situation on Pd/A. Having lower

TABLE 1: Results of Texture Characterizations for Pd-Supported Samples

samples	S_{BET} (m^2/g)		CZ lattice constant ^a (\AA)		Gaussian-fitting XRD (111) peak position (deg)		Pd particle diameter (nm)	
	fresh	aged	fresh	aged	fresh	aged	fresh	aged
Pd/CZ	55	12	5.403 ± 0.0009	5.400 ± 0.0014	28.61	28.63	1.5	6.1
(Pd/CZ) + A	147	45	5.404 ± 0.0002	5.399 ± 0.0008	28.60	28.64	1.4	7.5
(Pd/CZ) + (Pd/A)	141	47	5.403 ± 0.0002	5.391 ± 0.0012	28.60	28.68	1.5	7.5
(Pd/A) + CZ	142	43	5.397 ± 0.0000	5.389 ± 0.0001	28.62	28.69	5.0	7.8
CZ	56	10	5.393 ± 0.0000	5.383 ± 0.0005	28.65	28.74	—	—
Pd/A	220	51	—	—	—	—	5.7	7.9

^a Lattice constants are calculated by JADE 5, where the corresponding standard errors are also considered.

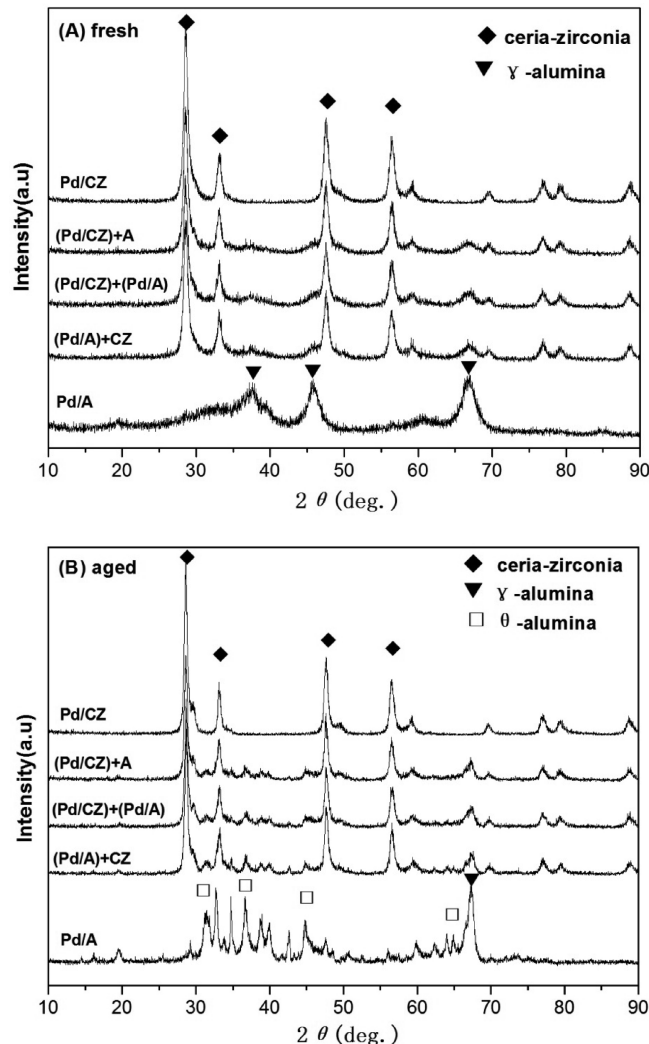


Figure 1. XRD patterns for (A) fresh and (B) aged Pd-supported samples.

surface areas and inferior thermal stability during aging, CZ-supported oxides still facilitate Pd dispersion on their interface more than that on alumina.

The overall shrinkage of CZ lattice constants was observed after aging, which is in line with the change of (111) reflection centers (Table 1).²³ Separation of larger Ce⁴⁺ ions from CZ to make slightly zirconia-rich main phases²³ and the transmission of Ce³⁺ (1.14 Å) to Ce⁴⁺ (0.97 Å) during high temperature lean treatment are the possible determining factors. However, the factors contributing to lattice shrinkage during hydrothermal aging are different from those gradual CZ lattice changes among the same group of samples. We observe a slight decrease in CZ lattice constant with the decline of Pd–CZ contacts in fresh

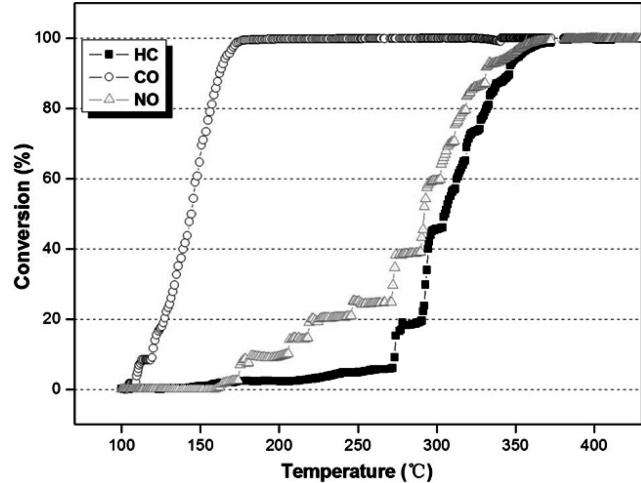


Figure 2. Representative TWC light-off curves for CO, NO, and C_3H_8 on Pd-supported catalysts.

and aged catalysts, where a concomitant weak shift of (111) reflection to lower angles was also observed. A higher Ce³⁺ content is more possible to be responsible for the shift³¹ rather than the ceria-rich main phase formation without additional severe treatment. Because of the lower redox potential of $\text{Pd}^{2+}/\text{Pd}^0$ than that of $\text{Ce}^{4+}/\text{Ce}^{3+}$, Pd particles may be inclined to easily maintain an oxidized state when in proximity with a CZ lattice [O] and activate the electrons on the Pd-supported interface, thus leaving CZ in trace-level reduced states or forming more oxygen vacancies.¹³ Smirnov et al. have already showed that vapor-deposited Pd films on a CZ substrate can completely oxidize under a 423 K ultrahigh vacuum condition.³² Substitutions of Ce⁴⁺ (0.97 Å) by Ce³⁺ (1.14 Å) in CZ supports, which enlarge the lattice constant, seemed to be promoted when Pd loaded. Our previous analysis also demonstrated the oxidized states of Pd particles on a CZ surface.²⁰

3.2. Light-Off Performance. Figure 2 shows the representative stoichiometric light-off behavior of CO, C_3H_8 , and NO conversions for all of the samples investigated. CO is oxidized at a much lower temperature than that of C_3H_8 . C_3H_8 and NO are converted almost in parallel, indicating the different catalytic process involved in that of CO oxidation. Different HCs may have different rate-determining steps concerning their oxidation, including surface adsorption, bond activation, and [O] supplying.³³ As the eliminations of NO and C_3H_8 require dissociation of molecules at the surface of the catalysts, their similar light-off behaviors imply that the overall reaction rate of C_3H_8 oxidation can be determined by C–H debonding. NO competes for oxidation, and the dissociated [O] may also fill the anionic vacancy, resulting in a complex response to reaction networks. Temperatures for 50% and 90% of exhaust conversion are listed in Table 2. CO oxidation activity is ordered as

TABLE 2: Temperatures Required for 50% and 90% Exhaust Conversion for Catalysts

	samples	CO (K)		C ₃ H ₈ (K)		NO (K)				
		T ₅₀	T ₉₀	ΔT ^a	T ₅₀	T ₉₀	ΔT ^a	T ₅₀	T ₉₀	ΔT ^a
fresh	Pd/CZ	416	443	27	578	619	41	564	604	40
	(Pd/CZ) + A	424	444	20	568	612	44	539	599	60
	(Pd/CZ) + (Pd/A)	436	458	22	554	592	38	550	583	33
	(Pd/A) + CZ	461	478	17	550	582	32	535	570	35
	Pd/A	482	502	20	546	575	29	517	558	41
aged	Pd/CZ	527	544	17	739	792	53	728	764	36
	(Pd/CZ) + A	544	594	50	711	758	47	698	736	38
	(Pd/CZ) + (Pd/A)	541	569	28	683	737	54	676	715	39
	(Pd/A) + CZ	536	556	20	660	714	54	663	705	42
	Pd/A	550	590	40	645	701	56	630	691	61

^a ΔT is defined as T₉₀ – T₅₀.

Pd/CZ > (Pd/CZ) + A > (Pd/CZ) + (Pd/A) > (Pd/A) + CZ > Pd/A. The Pd–CZ interface-containing catalysts promote CO conversion. The catalytic activity for NO reduction and parallel C₃H₈ oxidation is ordered as Pd/A > (Pd/A) + CZ > (Pd/CZ) + (Pd/A) > (Pd/CZ) + A ≈ Pd/CZ for fresh and aged samples, preferring the Pd–A interface-containing samples. The difference among CO conversion disappeared after the aging treatment, while the temperature gaps for NO and C₃H₈ were enlarged. These results indicate the different requirements for Pd-supported interface properties in specific exhaust conversions. Even for the so-called oxidation of CO and C₃H₈, the influence of the Pd support can be clearly differentiated, where the morphology, chemical states, and redox roles of the interfaces should be critical.

3.3. Oxygen Mobility. CO pulses with He intervals were employed to study the total oxygen storage capability (TOSC) of the catalysts at 500 °C (Figure 3), where 100% conversions for all exhausts were approached. CZ contents in catalysts roughly determined the overall TOSC amount. The Pd–CZ interface promotes the OSC activity to a higher level at 500 °C. In line with the previous conclusions, the quantified result shows that the improvement is not only related to the reduction of PdO but is also benefitted by Pd-supported contacts. Discrepant TOSC between Pd/CZ and Pd/A kept constant after aging. In contrast, TOSC activity for the other three samples is not differentiated much when compared with that of the corresponding fresh samples, indicating that one similar state of Pd-supported active sites may serve as an active location. Because of the consumption of lattice [O] from reducible CZ, the OSC difference among the samples eventually vanishes, along with the increase of CO pulses. An almost constant level of 0.05 mmol g⁻¹ OSC can be observed for the last several CO pulses. Boudouart reactions are most likely to take place under such an extremely rich condition especially without active lattice [O] supplied, where only 0.047 mmol g⁻¹ of OSC can be provided by even 100% reduction of PdO on 0.5 wt % Pd/A.

Figure 4 depicts the CO₂ response curves recorded in one CO–O₂ cycle at two frequencies. Two groups of CO₂ peaks are observed in both cases. A lean–rich frequency at 0.05 Hz provides better resolution of the peaks, which minimizes the errors for further quantification. The first group of CO₂ peaks is mainly attributed to direct CO oxidation by [O]. The second group of peaks is observed under the injection of O₂, and MS-DRIFTS analysis³⁴ demonstrated the formation of this group of CO₂ was mainly related to the oxidation of preadsorbed CO. Limited amount of CO₂ and carbonates on the surface of the material are also possible contributing factors.

DOSC data are reported in Table 3. The effect of the Pd–CZ and Pd–A interfaces in lean–rich oxygen buffering shows the

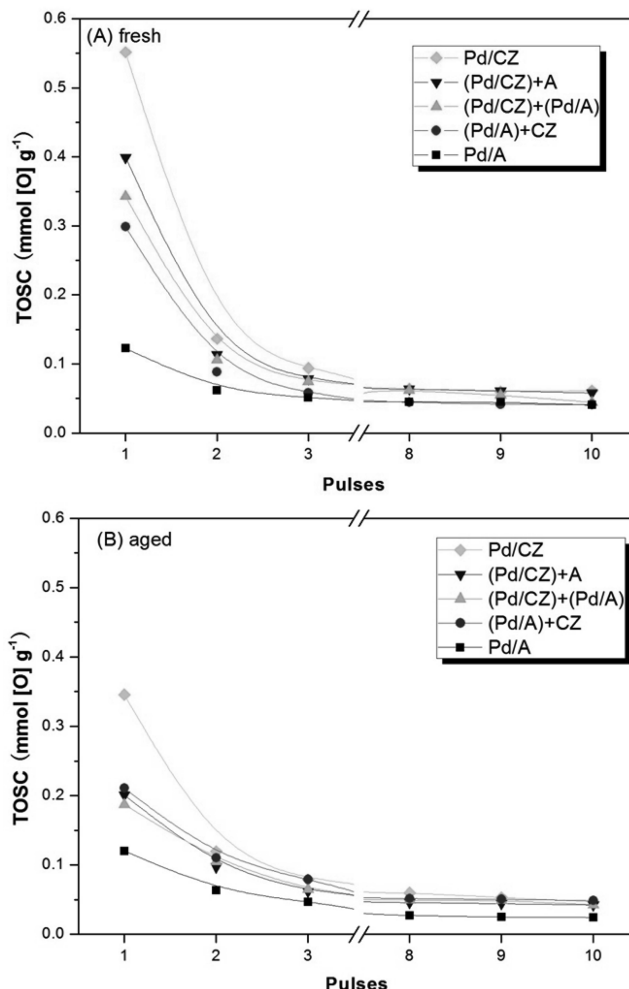


Figure 3. TOSC results of (A) fresh and (B) aged Pd-supported samples with successive 4% CO/1% Ar/He and pure He pulses at 773 K.

same trend as that of the TOSC analysis. A more drastic increase has been observed for the DOSC of (Pd/A) + CZ when temperatures increase. Another source of OSC besides the Pd/CZ interactions has begun to serve as an oxygen buffer at higher temperatures, indicated by the changes of OSC for fresh CZ. DOSCs of fresh Pd/A and (Pd/A) + CZ begin to be differentiated at 573 K, which is also the common temperature for Ce_{0.7}Zr_{0.3}O₂ to display OSC activity in H₂–TPR.⁸ However, without Pd loaded, OSC for severely aged CZ can be very limited, which is in line with our previous work. Instantaneous CO₂ production rates, after a certain amount of CO₂ produced

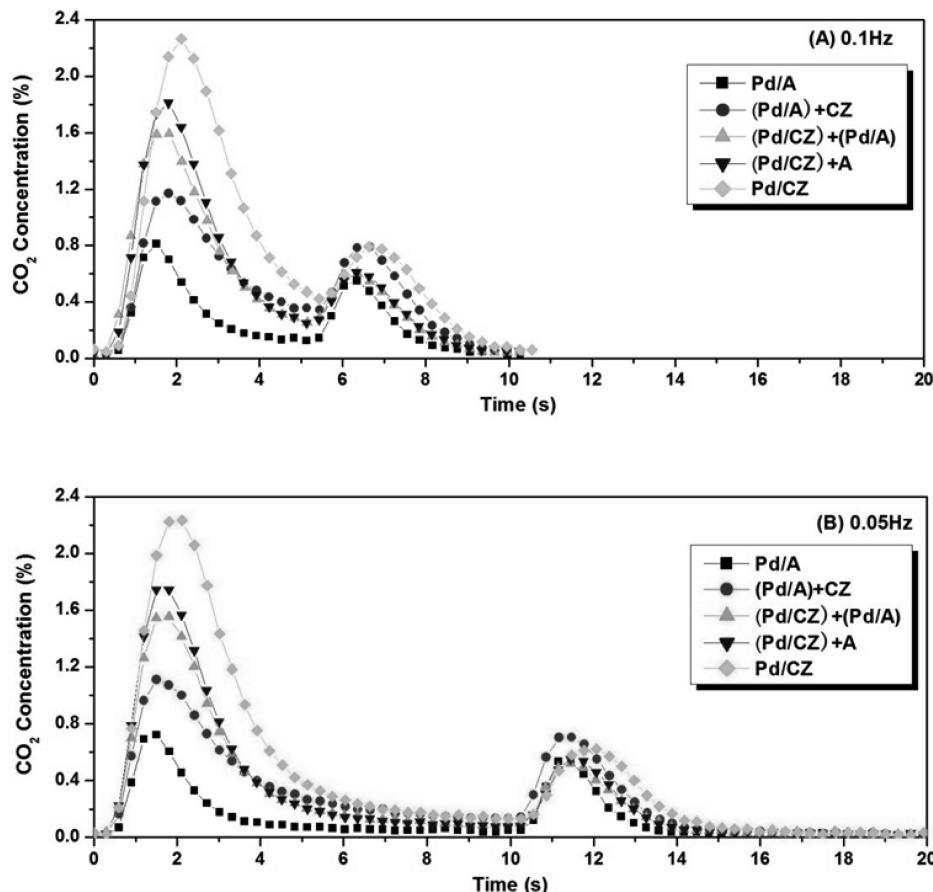


Figure 4. Representative CO₂ response curves at 773 K under (A) 0.1 Hz and (B) 0.05 Hz transient CO–O₂ measurements.

TABLE 3: DOSC of Fresh and Aged Pd-Supported Samples under a 0.05 Hz CO–O₂ Trasient Mode

		DOSC ($\mu\text{mol} [\text{O}] \text{ g}_{\text{catalyst}}^{-1}$)			
samples		473 K	573 K	673 K	773 K
fresh	Pd/CZ	399	600	711	746
	(Pd/CZ) + A	365	493	515	521
	(Pd/CZ) + (Pd/A)	275	382	463	496
	(Pd/A) + CZ	138	241	397	488
	Pd/A	105	215	248	236
	CZ	29	161	351	715
	Pd/CZ	247	458	665	728
	(Pd/CZ) + A	179	297	432	476
aged	(Pd/CZ) + (Pd/A)	168	251	399	462
	(Pd/A) + CZ	170	242	380	429
	Pd/A	61	136	186	213
	CZ	8	23	53	220

during CO injection, were calculated according to the equation below³⁵

$$\frac{\int_{t_0}^{t_i} \text{CO}_2 \text{ signal}}{t_i - t_0} = \text{rate} [\mu\text{mol of CO}_2/\text{sec}] \quad (1)$$

The $\int_{t_0}^{t_i} \text{CO}_2 \text{ signal}$ is the integrated peak area from t_1 to t_0 , where the gap between t_0 and t_1 is limited to 1 s. Apparent activation energies E_a for CO oxidation on the catalysts were calculated based on the Arrhenius equation, and the results are illustrated in Figure 5. The evolution of E_a explains the trend in TOSC and DOSC results. A Pd–CZ contact ensures the activation energy maintains even a significant amount of CO₂ produced without O₂ at the low and constant level, while the

activation energy for a Pd/A system in acquiring [O] increases drastically when little CO₂ is produced. CZ alone has an even worse oxidation activity than Pd/A due to higher E_a . However, the oxygen release capability of CZ can be greatly promoted by Pd loaded on or at higher temperatures. The Pd/CZ oxidation role is limited by the increasing E_a induced by less availability of reducible CZ. The aging treatment increases the E_a at every stage of OSC in all samples except (Pd/A) + CZ and also brought about similar evolution of E_a in samples with mixed supports, indicating a similar chemical environment for oxygen mobility.

3.4. In Situ DRIFTS Study. Groups of DRIFTS analyses were carried out to study the Pd-supported interfaces concerning the following issues: (1) surface states of Pd-supported interfaces for the catalysts, (2) extent of Pd-supported interactions for the oxygen buffering effect, and (3) role of the Pd-supported interfaces for TWC reactions.

Figures 6 and 7 illustrate the CO DRIFTS spectra for fresh and aged Pd-supported samples. The spectra generally show the increasingly intensified features assigned to CO₂ (g) in the region of 2400–2300 cm⁻¹ when heated. The intensity of these CO₂ (g) peaks agrees with the order of CO light-off and OSC behaviors but shows a negative correlation with NO and C₃H₈ conversions. Bands in the region of 1800–2200 cm⁻¹ attributed to carbonyls adsorption on different Pd sites and is noteworthy for discerning the in situ chemical roles of Pd-supported interfaces. Overlaps of CO (g) features, showing two symmetrical bands at 2120 and 2170 cm⁻¹, have been subtracted from all spectra, and the evolution of carbonyls adsorption on Pd sites can be tracked in higher reliability. CO adsorbed on Pd²⁺ (2162 cm⁻¹), Pd¹⁺ (2110 cm⁻¹), and Pd⁰ sites, including

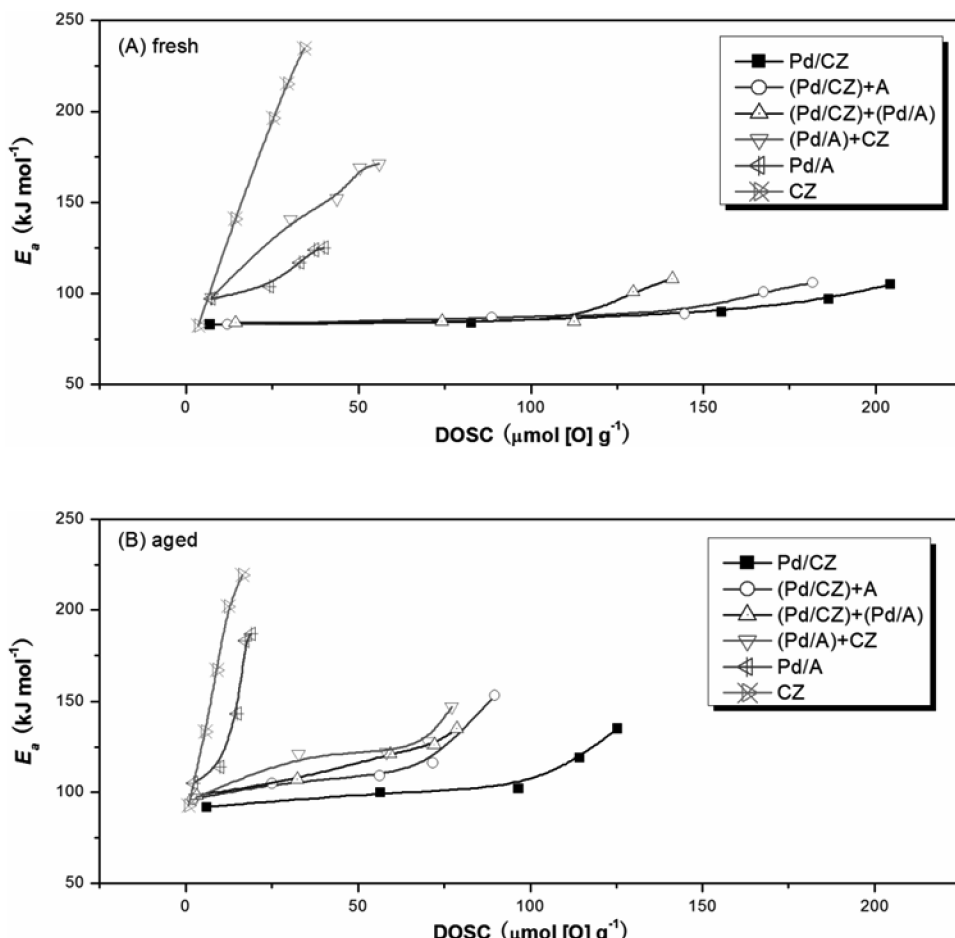


Figure 5. Apparent activation energies E_a for (A) fresh and (B) aged Pd-supported samples along with the increasing amount of OSC consumed.

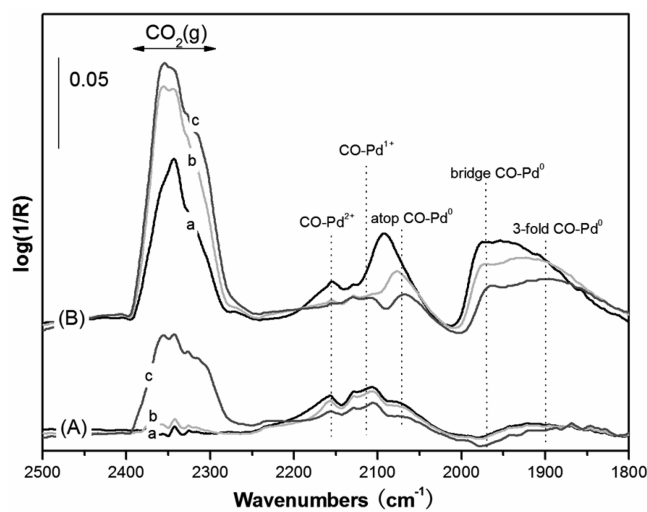


Figure 6. CO DRIFTS for (A) fresh Pd/A and (B) fresh Pd/CZ at (a) 303 K, (b) 383 K, and (c) 463 K. All samples were pretreated at 573 K in the vacuum condition of 10^{-4} Pa for 20 min. CO (0.02 MPa) was injected after the chamber was cooled to 303 K and stabilized for 20 min.

atop (2097–2060 cm^{-1}), bridge (1980–1970 cm^{-1}), or/and 3-fold (1900–1850 cm^{-1}) types, could be observed.^{17,18,36} Hydrothermal aging did not eliminate the overall difference between the adsorption behavior on Pd/CZ and Pd/A, implying metal dispersion is not the only determining issue for CO adsorption and oxidation behaviors.

Different Pd-supported interfaces remarkably modify the CO adsorption and oxidation behaviors. With an increase in temperature, an increase in CO_2 band intensity is accompanied with

a decline of CO adsorption over Pd^{2+} and Pd^{1+} sites, indicating the consumption of $[\text{O}]$ in initially oxidized Pd particles. Comparison between the spectra for Pd/A and Pd/CZ reveals similar CO adsorption manners on Pd^{n+} sites, although those on Pd/A are slightly weaker due to less metal accessibility or its concomitant barrier for efficient reduction. Thus, the different redox activities on Pd–A and Pd–CZ interfaces are expected to be mainly related to carbonyl adsorption on metallic Pd sites. Most evidence for Pd^0 -related adsorption is absent in Pd/A

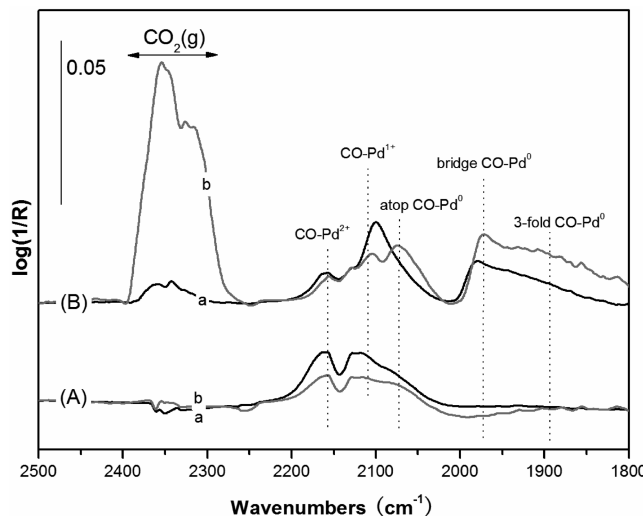


Figure 7. CO DRIFTS for (A) aged Pd/A and (B) aged Pd/CZ at (a) 303 K and (b) 463 K. The same experimental condition was applied as that in Figure 6.

samples, even though PdO particles are able to be reduced by CO at room temperature,^{17,18} and there is already some metallic Pd that exists on alumina surfaces.²⁰ Carbonyls adsorbed on Pd⁰ sites in Pd/CZ samples are very clear in fresh and aged states. The red shifts of atop, bridge, and 3-fold CO–Pd⁰ bands were induced by changes in adsorbed CO dipole coupling due to the effect of decreasing CO coverage brought about by the thermally favorable CO desorption and increasing CO catalytic conversion. For aged Pd/CZ, where less CO has been converted into CO₂, an even higher intensity of CO–Pd⁰ adsorption was recorded. The positive role of metallic Pd for catalytic CO oxidation can be justified, while evidence supporting Pd particles tends to maintain in oxidized states on CZ oxide before reactions have been observed.^{19,20} It is estimated that a Pd⁰ particle might act as a key active intermediate in dynamic Pdⁿ⁺/Pd⁰ redox couples during the reaction, but a static reduced metal might be better for molecule adsorption or bond activation. Moreover, lattice [O] and an anionic vacancy of CZ in proximate contact with Pd are the critical factors in influencing the redox activity of the catalyst.

A DRIFTS study was also applied to monitor the possible Pd-supported interface movements after 1223 K hydrothermal lean aging. In the case of fresh (Pd/CZ) + (Pd/A) (Figure 8A), Pd–CZ and Pd–A interfaces coexist and contribute to the CO adsorption and oxidation, bringing collected IR spectra intermediate shapes between that of Pd/CZ and Pd/A. Spectra for aged (Pd/CZ) + (Pd/A) are not differentiated much compared to their corresponding fresh states (Figure 8B). The attenuation of IR signals is mainly attributed to the sintering of the materials and the encapsulations of active sites after aging. The CO adsorption behaviors in aged (Pd/A) + CZ (Figure 8C) and (Pd/CZ) + A (Figure 8D) are noteworthy; they are very similar to that of the (Pd/CZ) + (Pd/A)-aged sample without any distinctive features such as was performed by Pd/CZ or Pd/A in Figure 7. The designed, fresh, exclusive Pd-supported interfaces are supposed to be substituted by the dual interfaces, showing no clear preference to stay as Pd/CZ or Pd/A during high-temperature lean treatment.

CO DRIFTS in gas flow for fresh and prereduced Pd/CZ samples were compared (Figure 9) in order to investigate the chemical evolution of the Pd–CZ interface, along with the gradual depletion of the unique oxidation activity. Prereduction in 5% H₂/He at 353 K for 30 min is a small possibility for

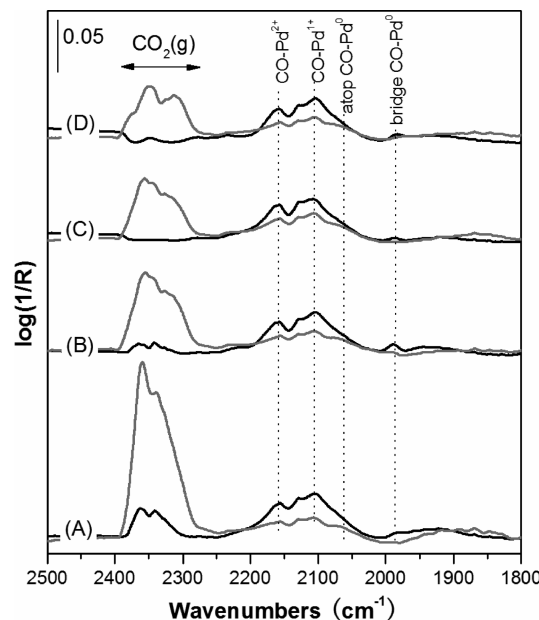


Figure 8. CO DRIFTS spectra for (A) fresh (Pd/CZ) + (Pd/A), (B) aged (Pd/CZ) + (Pd/A), (C) (Pd/A) + CZ, and (D) (Pd/CZ) + A at 303 K (black) and 463 K (gray). The same experimental condition was applied as that in Figure 6.

inducing the SMSI effect.³⁷ Changes in the IR spectra in prereduced Pd/CZ (Figure 9 B) were the consequence of [O] consumption in the catalyst. Compared with the DRIFTS spectra of fresh Pd/CZ in a vacuum system, similar band evolutions have been observed in Figure 9. Weaker intensities for all features are mainly attributed to different experimental conditions and lower gas concentrations to establish the adsorption equilibrium in the flowing gases. Prereduced Pd/CZ shows obviously different CO adsorption and oxidation behaviors, along with increasing temperatures, demonstrating the critical role of lattice [O] in modifying active metallic Pd sites.

Regarding the evolution of CO₂(g) features, which are found to correlate positively with CO oxidation activity, unreduced Pd/CZ clearly performs better oxidation activity during the whole process. The CO₂ bands quickly approached a constantly high level until 463 K. In contrast, the evolution of CO₂ bands of prereduced Pd/CZ displayed a volcano shape with increasing testing time. The phenomenon indicates less [O] could be supplied after reduction, although lattice [O] mobility is expected to be improved at higher temperatures. Moreover, repeated experiments recorded weaker CO₂ bands at 323 K than those at 303 K. CO₂ generation in 303–323 K is attributed to the initial reduction of PdO followed by [O] release from a near-surface Pd–CZ interface. In the case of prereduced Pd/CZ, Pd particles initially maintained oxidized states, thus facilitating CO oxidation at room temperature. However, as a significant amount of [O] in the catalyst had already been consumed, active [O] in a Pd–CZ interface or CZ bulk was not adequate enough for CO oxidation at low temperatures; unable to compensate, the consumed oxygen belonged to the original Pd particles.

Regarding the evolution of carbonyls adsorption on Pd sites, CO adsorption on Pd²⁺ and Pd¹⁺ shows a gradual decreasing intensity with an increasing testing time for both samples. Because of the lower [O] content in the material, the intensities of these bands for prereduced Pd/CZ appeared to be weaker than those of fresh Pd/CZ. Considering the adsorption on metallic Pd sites, because of the lower adsorption energy required,¹¹ atop CO–Pd⁰ sites quickly became indiscernible for

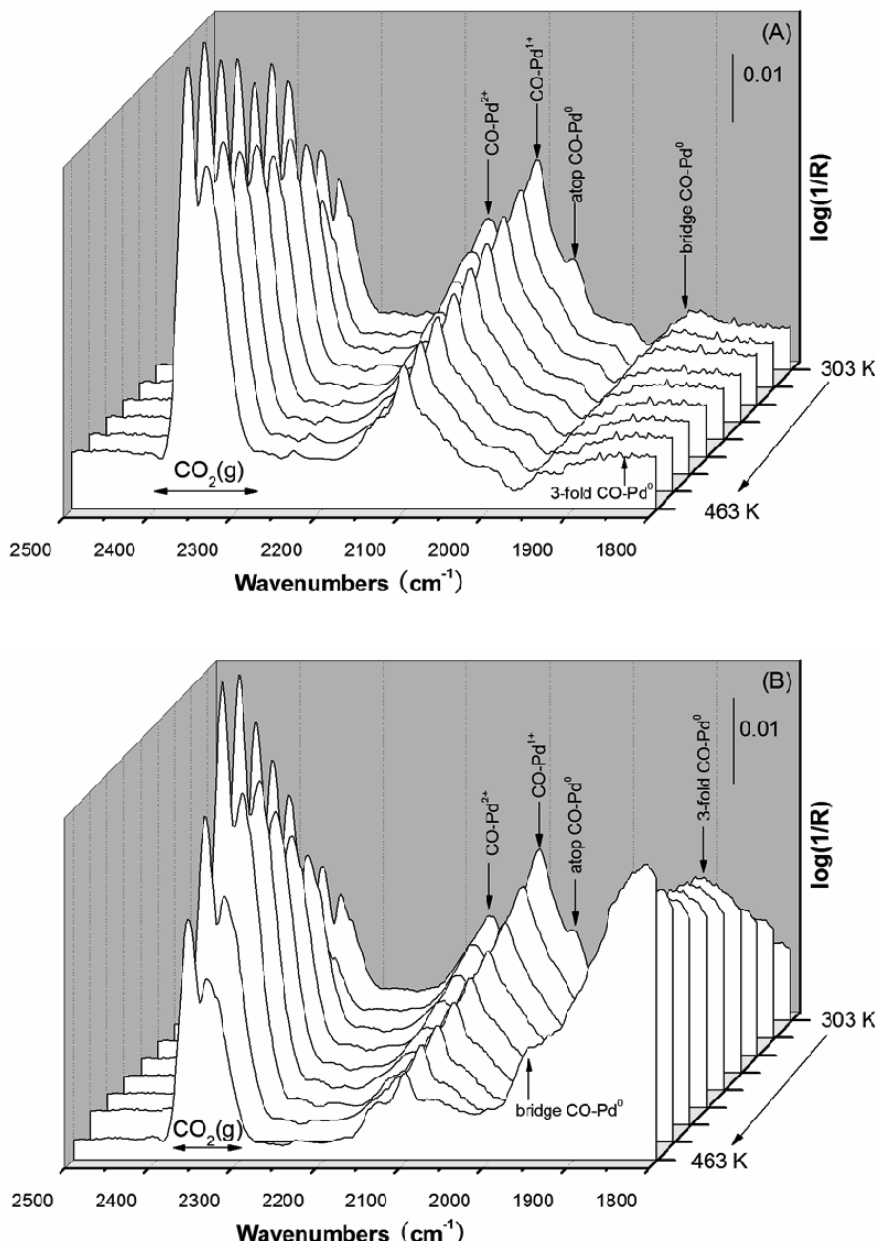


Figure 9. CO DRIFTS spectra for (A) fresh Pd/CZ and (B) prerduced Pd/CZ treated in 5% H₂/He with a flow rate of 200 mL min⁻¹ for 30 min at 353 K. Spectra were collected after purging the samples in 200 mL min⁻¹ N₂ at 773 K for 3 h and subsequently introducing 4% CO/He with a flow rate of 200 mL min⁻¹ from 303 to 463 K at an interval of 20 K.

both samples and shifted toward the CO adsorptions at lower wavenumbers. In the case of fresh Pd/CZ, the appearances of bridge CO–Pd⁰ and 3-fold CO–Pd⁰ are only marginally detected. Whereas in prerduced Pd/CZ, the signals attributed to these two sites are very clear soon after the light-off from 303 K. As the samples show quite similar adsorption in 2200–2000 cm⁻¹, contributions from thermal desorption and possible lower CO concentration should be largely excluded. With less [O] that could be supplied from CZ lattices near Pd particles, the exposure of a larger amount of metallic sites became the dominating impact, which could not manage to utilize the [O] in order to turn into oxidized states and directly participate CO oxidation. It is of interest to note the stepped growth of bridge CO–Pd⁰ and 3-fold CO–Pd⁰ signals with increasing testing time for prerduced Pd/CZ. When CO₂ (g) band intensities increased from 303 K, parallel increasing intensities of the CO–Pd⁰ bands was observed, where a number of Pd particles were reduced and constantly stayed in metallic

states. When CO₂ (g) bands approached the highest intensity in the volcano-shaped evolution, intensities of these CO–Pd⁰ bands stably maintained a similar level at 363–423 K, indicating that an [O] mobility related chemical equilibrium among Pdⁿ⁺/Pd⁰ and Ce⁴⁺/Ce³⁺ was approached, where a constant amount of metallic Pd actively participated in C–O activation and oxidation. Further exposure to CO flow caused the end of the reversed oxygen spillover effect on Pd–CZ, indicated by declining CO₂ (g) band intensities at 423–463 K, where pronounced increases in bridge CO–Pd⁰ and 3-fold CO–Pd⁰ intensities were also recorded. Deeply reduced CZ oxide no longer facilitates the oxidation of the loaded Pd in proximity, and the pumping function of Pd in accelerating [O] mobility in CZ lattice works in vain.

Figure 10 shows the CO–NO–O₂ DRIFTS spectra, where the CO and NO concentrations were kept the same as those applied in the TWC light-off test. C₃H₈ was excluded because of its strong interference without intrinsic alternations.¹⁵ Con-

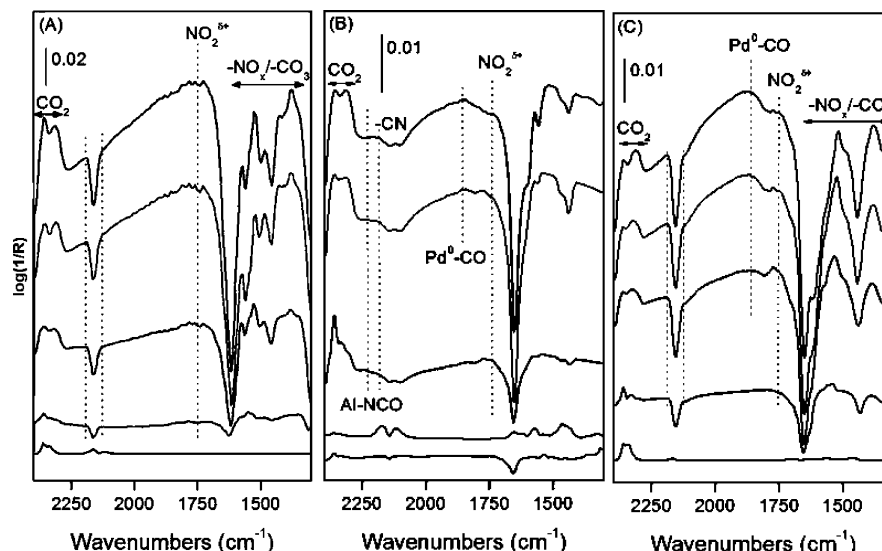


Figure 10. DRIFTS spectra for (A) fresh Pd/CZ, (B) Pd/A, and (C) (Pd/CZ) + (Pd/A) in a 200 mL min⁻¹ gas flow of 2% CO, 0.95% O₂, 0.1% NO (N₂ balance) at 323, 423, 523, 623, and 723 K from bottom to top. Spectra were collected after treating the sample in a 200 mL min⁻¹ gas flow of 2% CO, 0.95% O₂, 0.1% NO (N₂ balance) from room temperature to 773 K, reduced by 5% H₂, oxidized by 5% O₂ for 20 min at 573 K, and finally outgassed by N₂ to room temperature and stabilized for 20 min.

tributions of gaseous CO and NO were not subtracted because of complex reaction conditions, but the evolution of the IR features may provide an overall trend in surface adsorption behaviors. Evidence for NO adsorption and reduction is not evident due to its low adsorption coefficient and concentration in the feed gas,³⁸ while the overall intensity for the spectra declines greatly compared with the previous ones, suggesting the mutual interference of all gas components during their conversion. CO adsorptions on Pdⁿ⁺ sites in 2170–2110 cm⁻¹ are easier for tracking in Pd–CZ-containing samples. Steep features in the range of 1700–1300 cm⁻¹ appeared along with the reactions, where surface carbonates³⁹ and nitrites species⁴⁰ adsorbed onto support oxide surfaces overlapping each other may contribute to this. The possibility of the latter should be greatly limited because of the stoichiometry applied. On alumina with high surface acidity, adsorption of acidic molecules should be more difficult regardless of carbonates or nitrites. In the 1970–1750 cm⁻¹, the peaks are assigned to CO–Pd⁰, $-\text{NO}_x^{\delta+}$, and coordinated $-\text{C}=\text{O}$ “organic carbonates” on support oxides.⁴¹ Similarly, contributions of carbonate formation on alumina should be minor. It is therefore deduced that the metallic Pd–CO bond could be more easily maintained on Pd/A, while stronger Pdⁿ⁺–CO sites existing in Pd–CZ interface-containing samples running in parallel with a $-\text{NO}_x^{\delta+}$ signal represent the unreduced NO adsorbates. NCO species (2240–2211 and 2160–2154 cm⁻¹) formed by N–O dissociation and subsequent bonding with CO at Pd-supported interfaces is an important path for NO reduction,^{39,42} which is followed by decomposition to produce $-\text{CN}$ around 2164 cm⁻¹, along with increasing Pd⁰–CO adsorption. These fingerprints are marginally detected in Pd/CZ. The evidence is in line with the light-off results concerning NO and C₃H₈ conversions. The strong oxidative role of a Pd–CZ interaction and even oxidation of support oxides hinder NO dissociation and subsequent reduction by CO–NO–O₂ reaction networks.

4. Discussion

4.1. Features of Pd-Supported Interactions. Proximate interfacial contact between Pd and CZ induced lattice expansion of CZ because of the oxidative role of Ce⁴⁺ in CZ supports in

maintaining the oxidized states of loaded Pd particles on as-prepared samples (Table 1). As an [O] supplier and electron acceptor, oxidized Pd particles promote continuous CO oxidation profoundly under 573 K (Table 3). Recent research work has also pointed out the positive role of an active PdO core rather than metallic Pd layers for oxidation capability in ex situ conditions.¹⁹ Providing that higher Pd dispersion and a higher amount of PdO_x are positive for oxidation, even a 100% reduction of PdO could not explain the ease of CO oxidation in large quantities on Pd/CZ. Similar shapes of the second CO₂ formation peaks during an O₂ purge exclude the significant contribution from Boudouart reactions. The effect of CZ in continuous low-temperature redox reactions should be addressed.

During in situ reactions, more metallic Pd sites in Pd/CZ present higher activity in CO oxidation, although Pd/A is more inclined to let the loaded Pd stay in reduced states according to our previous XPS and H₂–TPR investigations.²⁰ Fernández-García et al.¹⁷ reported that Pd–CZ interactions facilitate metallic Pd formation, which initiates electronic activation of the C–O bond by transferring electron density into antibonding $2\pi^*$ orbitals. Detection of a higher amount of metallic Pd sites during reactions is not a conflict to the favorable Pdⁿ⁺ formation directly used for CO oxidation at low temperatures. Continuous reactivation of the Pdⁿ⁺/Pd⁰ redox couple promoting CO oxidation is evident for prereduced Pd/CZ (Figure 9). The [O] mobility accelerated by intermediate metallic Pd sites is essential to CO oxidation, where Pd–CZ interfacial interaction plays a crucial role in low-temperature oxidations as OSC activity of CZ alone is greatly limited below 573 K.⁸

With the oxygen spilling back from the CZ lattice, oxidation activity of Pd has been greatly promoted. During the back spillover of oxygen, electrons received by Pd after CO oxidation are chemically favored to spill over into CZ supports and stabilize the Ce³⁺ formed after oxygen release. Reduced Pd particles therefore act as active intermediate species during CO oxidation. Metallic Pd performs adequate activity in CO adsorption and activation. It subsequently oxidizes carbonyl adsorbates when facilitated by lattice [O] released from CZ, where Pdⁿ⁺ may become noticeable in a limited number and relaxation time (Figures 6 and 7). Pd–CZ interaction-promoted

TABLE 4: Favorable TWC Reaction Pathways for Different Pd-Supported Interfaces Concerning CO and NO Conversions^a

Pd-supported interaction	possible reactions pathways
Pd-CZ strong	$\text{Ce}_{0.67}\text{Zr}_{0.33}\text{O}_2 + \text{Pd}(\text{s}) \longrightarrow \text{PdO}_x(\text{s}) + \text{Ce}_{0.67}\text{Zr}_{0.33}\text{O}_{2-x} + V_0$ $\text{PdO}_{x+y}(\text{s}) + x \text{H}_2(\text{g}) + y \text{CO}(\text{g}) \longrightarrow \text{Pd}(\text{s}) + x \text{H}_2\text{O}(\text{g}) + y \text{CO}_2(\text{g})$ $\text{PdO}_x(\text{s}) + x \text{H}_2(\text{g}) \longrightarrow \text{Pd}(\text{s}) + \text{H}_2\text{O}(\text{g})$ $\text{Ce}_{0.67}\text{Zr}_{0.33}\text{O}_{2-x} + V_0 + \text{PdO}_x(\text{s}) \longrightarrow \text{Pd}(\text{s}) + \text{Ce}_{0.67}\text{Zr}_{0.33}\text{O}_2$ $\text{Ce}_{0.67}\text{Zr}_{0.33}\text{O}_2 + x \text{H}_2(\text{g}) + y \text{CO}(\text{g}) \longrightarrow \text{Ce}_{0.67}\text{Zr}_{0.33}\text{O}_{2-x-y} + V_0 + x \text{H}_2\text{O}(\text{g}) + y \text{CO}_2(\text{g})$ $\text{Pd}(\text{s}) + x/2 \text{O}_2(\text{g}) \longrightarrow \text{PdO}_x(\text{s})$ $\text{Ce}_{0.67}\text{Zr}_{0.33}\text{O}_{2-x} + V_0 + x/2 \text{O}_2(\text{g}) \longrightarrow \text{Ce}_{0.67}\text{Zr}_{0.33}\text{O}_2$ $\text{Pd}(\text{s}) + (x+y)\text{NO}(\text{g}) + \text{Ce}_{0.67}\text{Zr}_{0.33}\text{O}_{2-x} + V_0 \longrightarrow \text{PdO}_y(\text{s}) + \text{Ce}_{0.67}\text{Zr}_{0.33}\text{O}_2 + (x+y)/2 \text{N}_2(\text{g})$ $\text{Pd}(\text{s}) + (x+y) \text{NO}(\text{g}) + x \text{CO}(\text{g}) \longrightarrow \text{PdO}_y(\text{s}) + x \text{CO}_2(\text{g}) + (x+y)/2 \text{N}_2(\text{g})$
Pd-A strong	$\text{Pd}(\text{s}) + x \text{NO}(\text{g}) \longrightarrow \text{PdO}_x(\text{s}) + x/2 \text{N}_2(\text{g})$

^a Effects of WGS producing H₂ are taken into consideration. In each reaction equation, $x > y > 0$. V_0 stands for ceria-related surface oxygen vacancies. The Boudouard reaction has a low possibility in TWC reactions.

[O] mobility is kinetically corroborated (Figure 5). In brief, [O] in PdO is easier for low temperature release but limited by the Pd loading ratio. As the compensating [O] resource, abundant lattice [O] in CZ migrates subsequently at higher E_a . The combination of Pd and CZ lowers E_a , while increasing [O] mobility. Such redox couples between Pd and support oxides do not work for alumina, thus lowering the oxidation capability of Pd/A.

A recent study by EDS has precisely revealed the tendency of Pd particles to contact with CZ materials more than alumina, when CZ and Pd were impregnated on alumina after calcination at 773 K.¹⁷ However, under more severe conditions, for samples hydrothermally aged at 1223 K for 10 h, we observe Pd particles inclined to be randomly dispersed on the mechanically mixed supports. This is corroborated by the combination of DRIFTS spectra, E_a of DOSC, and NM dispersion of aged (Pd/CZ) + (Pd/A), (Pd/CZ) + A, and (Pd/A) + CZ, which meets the principle of entropy increase. Wynblatt et al. have reported the faster sintering of noble metals via vapor phase transport as volatile oxides, while the NM particles move more slowly as metallic atoms or clusters under moderate conditions,⁴³ where the preference of chemical interaction between Pd and support can be more dominated. Therefore, high-temperature lean treatment seems to be the main driving force for the nonpreferable Pd movements. Pd-supported interfaces can be redistributed during real applications, and the preparation procedure initiated by Fernández-García et al.¹⁷ can be a desirable way to maintain a stable Pd–CZ contact under severe conditions.

4.2. Limits of Redox Activity in Pd–CZ Interfaces. Contributed by the oxygen spillover effect on Pd–CZ interface, samples with Pd–CZ interaction show more desired activity in CO conversion and serving as the quick responding buffer to the oscillating A/F ratios. This promotion role is limited by increasing reaction temperatures and CZ reducing extents, both of which are related to the intrinsic properties of CZ.

DOSCs of fresh Pd/A and (Pd/A) + CZ begin to be differentiated at 573 K (Table 3) due to the direct OSC contribution from CZ. CZ materials without Pd proximity can also release their lattice [O], participating CO oxidation at higher temperatures. Three fresh samples with mixed supports perform more similar OSC with increasing temperatures, indicating the

determining role of CZ contents for high-temperature CO oxidation. At higher temperatures, the advanced OSC performance of sample Pd/CZ is more dependent on the one time higher CZ content rather than the Pd–CZ interactions. Nevertheless, without the spillover motivation from anchored Pd on CZ, E_a for oxygen releasing from CZ alone is greatly limited, even at very low reducibility (Figure 5). In this regard, the oxidative effect from a Pd–CZ interaction appears to be practically essential for DOSCR and TWC applications, especially under low-temperature light-off conditions.

The absence of a remarkable difference in TOSC during the last several CO–He pulses (Figure 3) and the ascending E_a (Figure 5) during OSC consuming implies Pd loaded on CZ exerts a limited effect to bulk oxygen release. Bulk reducibility of CZ is thermodynamically controlled by the theoretical reducibility from CeO₂ to Ce₂O₃. When the reduction degree is approaching 25%, the OSC advantages of CZ and Pd/CZ are gradually depleted, accompanying the stepwise deactivation of the oxygen back spillover effect on a Pd–CZ interface (Figure 9). Consequently, the formation of CO₂ drops, leaving more metallic Pd exposed without CO oxidation activity. Concerning the texture of bulk ceria–zirconia, the presence of oxygen vacancies is another driving force for bulk [O] migration and release. It is supposed that the diffusion of [O] from the bulk to the surface by the oxygen concentration gradient would largely determine the OSC performance of ceria-based materials.^{8,25} Hori et al. proposed that an excessive amount of anionic vacancies in the lattice limits further reduction of bulk-structured ceria materials.⁴⁴ In CO–He pulse measurements, the creation of excessive oxygen vacancies hinders the bulk [O] migration of CZ. E_a data agrees with the TOSC results: when 1 g of fresh (Pd/CZ) + A releases more than 50 μmol [O] to that of (Pd/A) + CZ, their instantaneous E_a comes to a similar level and shows no further difference in the TOSC test.

4.3. Impacts of Pd-Supported Interactions for TWC Reactions. Redox features and morphologies of Pd-supported interfaces greatly determine TWC performance. CO conversion is positively correlated with Pd–CZ promoted C–O bond activation and oxidation. Because of the lower redox potential of Pd²⁺/Pd⁰ than that of Ce⁴⁺/Ce³⁺, Pd proximity facilitates oxygen back spillover and oxygen spillover on CZ, forming an

oxygen equilibrium between lattice [O] and gas phase O₂. Therefore, in contrast with the situation for Pd/A, the overall CO oxidation rate on Pd/CZ is not determined by activation of gas phase O₂ through a L–H type pathway. NO reduction is a structure-sensitive reaction, which prefers to be dissociated and recombined into N₂ on reduced Pd with a larger particle size.¹⁶ Loaded on acidic Al₂O₃, the Pd⁰ state is more easily maintained even at high oxygen concentrations.³⁸ Without the oxygen spillover effect in Pd–CZ, a lower chance of oxygen activation happens on the Pd/A interface, and thus the competence of [O] in occupying metallic Pd sites has been attenuated to some extent, which in turn promote the adsorption and dissociation of NO and concomitant electron transfer. Fernández-García et al.¹⁸ have shown the improvement of NO reduction on catalysts with ceria–zirconia patches added on Pd/Al₂O₃ formulation. The improvement of NO dissociation facilitated by a large amount of ceria-related oxygen vacancies overcomes the strong oxidative activity from increasing [O] mobility. In our case, without the synergic effect of Pd–CZA in improving NO reduction, the exclusive existence of Pd/CZ performs a predominant oxidation role and depresses [O] activation from gas molecules, including NO and O₂. Partially reduced Pd particles are reported to be positive for C₃H₈ oxidation.⁴⁵ Because of the different oxidation rate-determining steps varying with HCs species,³³ a strong oxidative effect and specific morphology of Pd-supported interfaces may not be universally positive. In the case of C₃H₈ oxidation, steps of synchronous C–H and N–O dissociation seem to be more predominant than the simple HC oxidation by lattice [O] or activated O₂. Here, NO overwhelmingly competes with other oxygen resources and largely determines the C₃H₈ oxidation rate. Favorable TWC reactions on (Pd/CZ) + (Pd/A) systems are summarized in Table 4.

Morphology of Pd particles is another important factor. Pd dispersion is improved on ceria–zirconia, benefitting nonstructure sensitive reactions such as CO oxidation. However, larger Pd particles on alumina are desirable for NO and C₃H₈ conversions. During hydrothermal aging at 1223 K for 10 h, nonpreferable migrations of Pd-supported interfaces take place among the samples with CZ and alumina supports. However, in the case of TWC light-off tests, Pd-supported morphology is more important. Differences in CO conversion are almost diminished due to the drastic Pd particle aggregation and encapsulation induced by severe CZ sintering. Because of the higher surface area and better thermal stability of alumina, advantages for NO and C₃H₈ conversions are enlarged on Pd/A after aging.

5. Conclusions

By stepwise changing Pd-loading locations on ceria–zirconia and alumina, we investigated features and mechanisms of the catalytic roles of metal–support interface as well as their significance for oxygen buffers. The dynamic oxidative effect from Pd–CZ interaction, which is essential for improving [O] mobility, is limited by the reduction degree of CZ oxides as well as higher reaction temperatures. Loaded Pd particles can lower the activation energy for lattice [O] migration of CZ. However, deeply reduced CZ with a limited amount of mobile lattice oxygen caused the end of the oxygen back spillover effect on a Pd–CZ interface by lowering the reoxidation activity of metallic Pd. Different Pd-supported interfaces are selectively active for the conversion of a certain exhaust component. The larger particle size and reduced state of Pd on Al₂O₃ accelerates NO and C₃H₈ conversions, where the molecular bond dissociations on the surfaces of the catalysts become the rate-determining

steps. A strong oxidative Pd–CZ interface suppresses the dissociation of gas molecules in obtaining [O] and only promotes nonstructure-sensitive CO oxidation. Random interface redistribution and more severe Pd–CZ sintering take place after 1223 K hydrothermal lean aging. Pd-supported interfaces define different redox properties in improving the nondefinitely correlated oxygen-buffering effects and TWC performances.

Acknowledgment. The authors are grateful for the financial support from the Program of New Century Excellent Talents in University (NCET-06-0243), Program of Introducing Talents of Discipline to Universities of China (B06006), and Key program of Natural Science foundation of Tianjin (07JC-ZDJC01600).

References and Notes

- (1) Kašpar, J.; Fornasiero, P.; Hickey, N. *Catal. Today* **2003**, *77*, 419.
- (2) Gandhi, H. S.; Graham, G. W.; McCabe, R. W. *J. Catal.* **2003**, *216*, 433.
- (3) Bedrane, S.; Descorme, C.; Duprez, D. *Catal. Today* **2002**, *73*, 233.
- (4) Wu, X. D.; Yang, B.; Weng, D. *J. Alloy. Compd.* **2004**, *376*, 241.
- (5) Di Monte, R.; Kašpar, J.; Fornasiero, P.; Graziani, M.; Pazé, C.; Gubitos, G. *Inorg. Chim. Acta* **2002**, *334*, 318.
- (6) Aneggi, E.; Boaro, M.; de Leitenburg, C.; Dolcetti, G.; Trovarelli, A. *J. Alloy. Compd.* **2006**, *408*, 1096.
- (7) Shen, M. Q.; Wang, J. Q.; Shang, J. C.; An, Y.; Wang, J.; Wang, W. L. *J. Phys. Chem. C* **2009**, *113* (8), 1543.
- (8) Zhao, M. W.; Shen, M. Q.; Wang, J. *J. Catal.* **2007**, *248*, 258.
- (9) Hepburn, J. S.; Dobson, D. A.; Hubbard, C. P. *SAE Paper* **1994**, *2057*.
- (10) Di Monte, R.; Kašpar, J. *Top. Catal.* **2004**, *28*, 47.
- (11) Fernández-García, M.; Martínez-Arias, A.; Salamanca, L. N.; Coronado, J. M.; Anderson, A.; Conesa, J. C.; Soria, J. *J. Catal.* **1999**, *187*, 474.
- (12) Zhao, M. W.; Shen, M. Q.; Wang, J.; Wang, W. L. *Ind. Eng. Chem. Res.* **2007**, *46*, 7883.
- (13) Hu, Z.; Wan, C. Z.; Lui, Y. K.; Detting, J.; Steger, J. *J. Catal. Today* **1996**, *30*, 83.
- (14) Fornasiero, P.; Ranga Rao, G.; Kašpar, J.; L'Erario, F.; Graziani, M. *J. Catal.* **1998**, *175*, 269.
- (15) Martínez-Arias, A.; Hungria, A. B.; Fernández-García, M.; Iglesias-Juez, A.; Anderson, J. A.; Conesa, J. C. *J. Catal.* **2004**, *221*, 85.
- (16) Iglesias-Juez, A.; Martínez-Arias, A.; Fernández-García, M. *J. Catal.* **2004**, *221*, 148.
- (17) Fernández-García, M.; Martínez-Arias, A.; Iglesias-Juez, A.; Hungria, A. B.; Anderson, J. A.; Conesa, J. C.; Soria, J. *Appl. Catal., B* **2001**, *31*, 39.
- (18) Fernández-García, M.; Martínez-Arias, A.; Iglesias-Juez, A.; Hungria, A. B.; Anderson, J. A.; Conesa, J. C.; Soria, J. *Appl. Catal., B* **2001**, *31*, 51.
- (19) Winkler, P.; Dimopoulos, P.; Hauert, R.; Bach, C.; Aguirre, M. *Appl. Catal., B* **2008**, *84*, 162.
- (20) Shen, M. Q.; Yang, M.; Wang, J.; Wen, J.; Zhao, M. W.; Wang, W. L. *J. Phys. Chem. C* **2009**, *113* (8), 3212.
- (21) Nibelke, Rob, H.; Nievergeld, Arthur, J. L.; Hoebink, Jozef, H. B. J.; Marin, Guy, B. *Appl. Catal., B* **1998**, *19*, 245.
- (22) Descorme, R.; Taha, R.; Mouaddib-Moral, N.; Duprez, D. *Appl. Catal., A* **2002**, *223*, 287.
- (23) Daley, R. A.; Christou, S. Y.; Efsthathiou, A. M.; Anderson, J. A. *Appl. Catal., B* **2005**, *60*, 117.
- (24) Damyanova, S.; Perez, C. A.; Schmal, M.; Bueno, J. M. C. *Appl. Catal., A* **2002**, *234*, 271.
- (25) Wang, J.; Wen, J.; Shen, M. Q. *J. Phys. Chem. C* **2008**, *112*, 5113.
- (26) Rogemond, E.; Essayem, N.; Fréty, R.; Perrichon, V.; Primet, M.; Chevrier, M.; Gauthier, C.; Mathis, F. *Catal. Today* **1996**, *29*, 83.
- (27) Gatica, J. M.; Baker, R. T.; Fornaseiro, P.; Bernal, S.; Kašpar, J. *J. Phys. Chem. B* **2001**, *105*, 1191.
- (28) Yamauchi, M.; Ikeda, R.; Kitagawa, H.; Takata, M. *J. Phys. Chem. C* **2008**, *112*, 3294.
- (29) Falkowski, M.; Novakowski, R.; Holyst, R. *J. Phys. Chem. C* **2004**, *108*, 7373.
- (30) Dawody, J.; Eurenus, L.; Abdulhamid, H.; Skoglundh, M.; Olsson, E.; Fridell, E. *Appl. Catal., A* **2005**, *296*, 157.
- (31) Deganello, G.; Giannici, F.; Martorana, A.; Pantaleo, G.; Prestianni, A. *J. Phys. Chem. B* **2006**, *110*, 8731.
- (32) Smirnov, M. Y.; Graham, G. W. *Catal. Lett.* **2001**, *72*, 39.
- (33) Zhao, S.; Gorte, R. J. *Appl. Catal., A* **2004**, *277*, 129.

- (34) Mondelli, V.; Dal Santo, V.; Trovarelli, A.; Boaro, M.; Fusi, A.; Psaro, R.; Recchia, S. *Catal. Today* **2006**, *113*, 81.
- (35) Hori, Carla, E.; Brenner, A.; Simon Ng, K.Y.; Rahmoeller, Kenneth, M.; Belton, D. *Catal. Today* **1999**, *50*, 299.
- (36) Changho, J.; Hideyuki, T.; Michihisa, K.; Momoji, K.; Ewa, B.; Akira, M. *Catal. Today* **2006**, *111*, 322.
- (37) Frolova, Elena, V.; Ivanovskaya, Marya, I.; Hlushonak, Henadz, K. *Opti. Mater.* **2006**, *28*, 660.
- (38) Fernández-García, M.; Iglesias-Juez, A.; Martínez-Arias, A.; Hungría, A. B.; Anderson, J. A.; Conesa, J. C.; Soria, J. J. *Catal.* **2004**, *221*, 594.
- (39) Fan, J.; Weng, D.; Wu, X. D.; Wu, X. D.; Ran, R. *J. Catal.* **2008**, *258*, 177.
- (40) Symalla, M. O.; Drochner, A.; Vogel, H.; Philipp, S.; Göbel, U.; Müller, W. *Top. Catal.* **2007**, *42*–43, 199.
- (41) Prinetto, F.; Ghiotti, G.; Nova, I.; Lietti, L.; Tronconi, E.; Forzatti, P. *J. Phys. Chem. B* **2001**, *105*, 12732.
- (42) Abdulhamid, H.; Dawody, J.; Fridel, E.; Skoglundh, M. *J. Catal.* **2006**, *244*, 169.
- (43) Wynblatt, P.; Gjostein, N. A. *Prog. Solid State Chem.* **1975**, *9*, 21.
- (44) Hori, C. E.; Permana, H.; Ng, K. Y. S.; Brenner, A.; More, K.; Rahmoller, K. M.; Belton, D. *Appl. Catal., B* **1998**, *16*, 105.
- (45) Yazawa, Y.; Yoshida, H.; Takagi, N.; Komai, S.; Satsuma, A.; Hattori, T. *J. Catal.* **1999**, *187*, 15.

JP810904D